A Linear Stochastic Model of a GCM's Midlatitude Storm Tracks

YUNQING ZHANG

Program in Atmospheric and Oceanic Sciences, Princeton University, Princeton, New Jersey

ISAAC M. HELD

NOAA/Geophysical Fluid Dynamics Laboratory, Princeton, New Jersey

(Manuscript received 26 February 1998, in final form 6 October 1998)

ABSTRACT

A linear stochastic model is used to simulate the midlatitude storm tracks produced by an atmospheric GCM. A series of six perpetual insolation/SST GCM experiments are first performed for each month. These experiments capture the ''midwinter suppression'' of the Pacific storm track in a particularly clean way. The stochastic model is constructed by linearizing the GCM about its January climatology and finding damping and stirring parameters that best reproduce that model's eddy statistics. The model is tested by examining its ability to simulate other GCM integrations when the basic state is changed to the mean flow of those models, while keeping the stirring and damping unchanged.

The stochastic model shows an impressive ability to simulate a variety of eddy statistics. It captures the midwinter suppression of the Pacific storm track qualitatively and is also capable of simulating storm track responses to El Niño. The model results are sensitive to the manner in which the model is stirred. Best results for eddy variances and fluxes are obtained by stirring the temperature and vorticity at low levels. However, a better simulation of the spatial structure of the dominant wave train as defined by covariance maps is obtained by stirring the temperature equation only, and at all levels.

1. Introduction

Understanding the distribution of eddy variances and fluxes due to baroclinic eddies remains one of the central concerns of dynamical meteorology. It is clear that linear theory has much to tell us about the midlatitude storm tracks, as indicated, for example, by the distribution of the ''local Eady growth rate,'' presented in Hoskins and Valdes (1990). Accepting the hypothesis that the dynamics linearized about the time-mean flow is of value, how does one best make use of it to develop a theory for storm track structure? Eigenmode analysis has been a common starting point (e.g., Frederiksen 1983), but it is not clear how to convert information about growing modal structures into time-averaged statistics.

Farrell and Ioannou (1996a,b) have pioneered an alternative approach in which a statistically steady state is modeled directly by assuming that nonlinearity can be replaced by two effects on the linear dynamics: damping and stochastic stirring. The resulting model resembles stochastic theories of homogeneous turbulence (Leith 1971), but because of the complexity of the inhomogeneous meteorological problem, one tries to proceed with much simpler expressions for the stirring and effective damping than is used in the turbulence literature. Farrell and Ioannou (1993a,b; 1994; 1995) have analyzed a variety of idealized flows, while Whitaker and Sardeshmukh (1997) have recently obtained very promising results with a two-layer balanced model.

While studying the seasonal cycle of the Northern Hemisphere storm tracks, particularly the ''midwinter suppression'' of the Pacific storm track (Nakamura 1992), we have been attracted to the stochastic modeling approach and have found it to be valuable. We first use a full primitive equation general circulation model in a series of perpetual insolation/perpetual SST experiments, which simulate the midwinter suppression phenomenon in a clear form. We then use a linearized, dry version of this GCM, linearized about the time-mean flows produced by these GCM experiments, to construct our stochastic models.

In section 2 the perpetual insolation/SST GCM and the climates it generates are described. The construction and tuning of the linear stochastic GCM is described in section 3. The linear stochastic model's performance in reproducing nonlinear eddy statistics is examined in section 4. In section 5 we concentrate on the model's sen-

Corresponding author address: Dr. Isaac M. Held, NOAA/GFDL, Princeton University, P.O. Box 308, Princeton, NJ 08542.
E-mail: ih@gfdl.gov

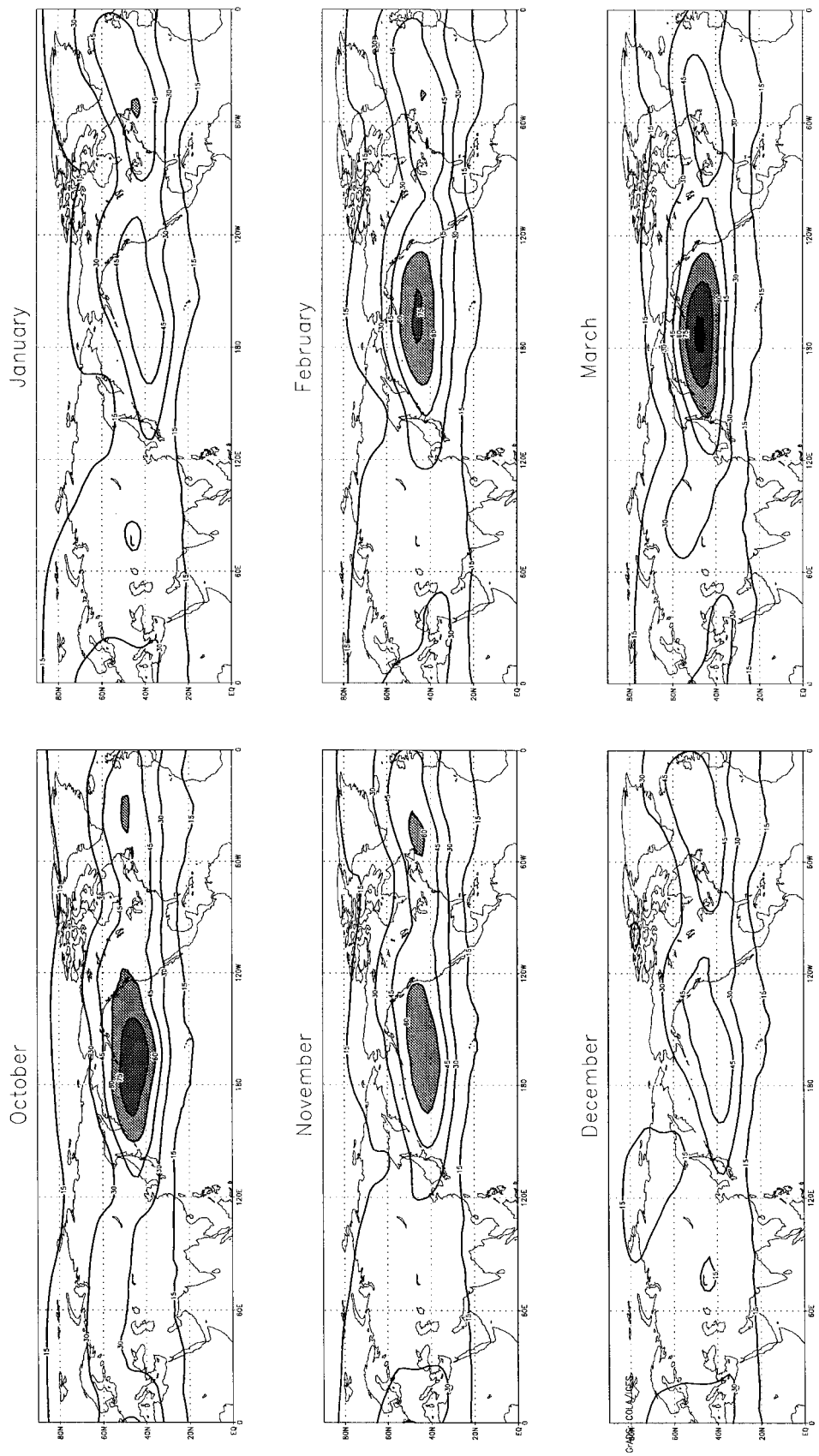

FIG. 1. The rms of bandpass-filtered geopotential height at 205 mb from the perpetual GCM. Contour interval: 15 m. Values larger than 60 m are shaded.

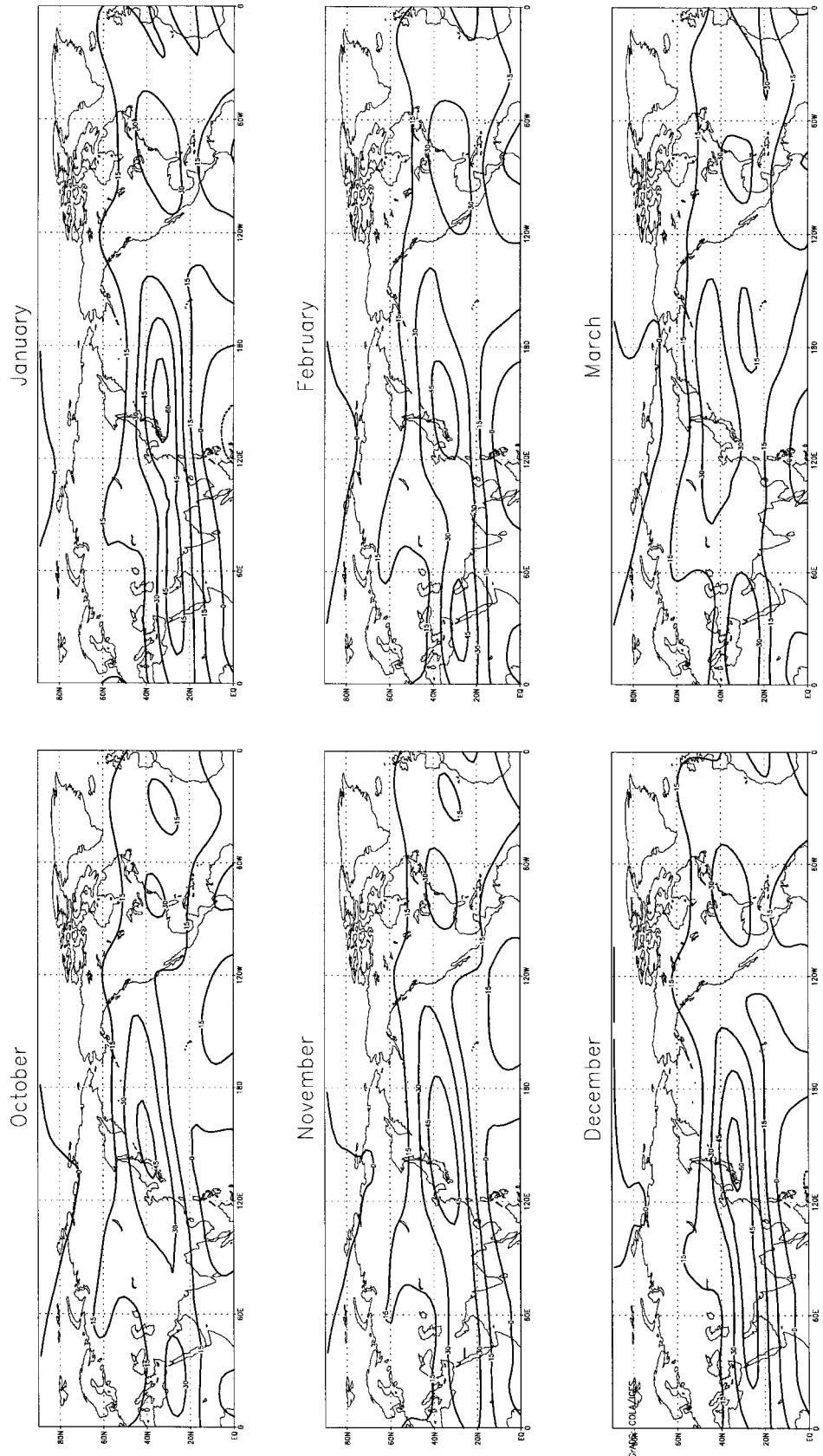

FIG. 2. Time-mean zonal wind at 205 mb from the perpetual GCM. Contour interval: 15 m s^{-1}.

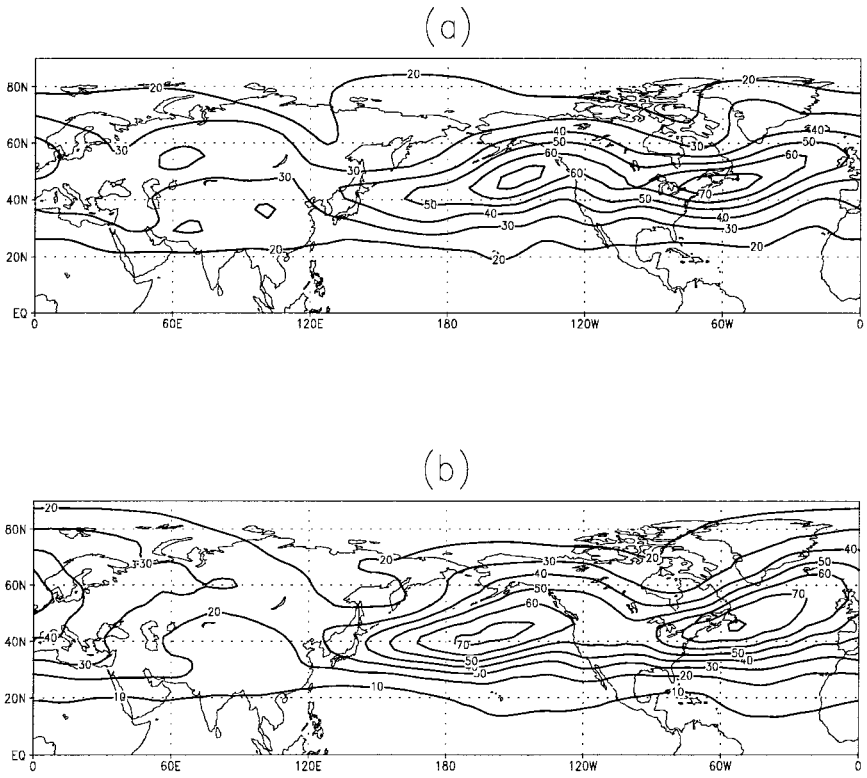

FIG. 3. The horizontal structures of the rms of the geopotential height at 350 mb from the linear model (a) and from the perpetual Jan run (b). Contour interval 10 m.

sitivity to the basic-state changes associated with the seasonal cycle and interannual variability. The results are summarized and discussed in section 6.

2. Perpetual insolation/SST GCM

Nakamura (1992) has drawn attention to the fact that the Pacific storm track attains its maximum strength in spring and autumn although the jet stream and the vertical wind shear over the Pacific are at maximum strength in midwinter. The midwinter suppression of the Pacific storm track is present in the seasonal GCM developed by the Climate Dynamics Group at the Geophysical Fluid Dynamics Laboratory (GFDL) and in other models (Christoph et al. 1997). Rather than study this seasonally varying model, we have performed a series of GCM integrations with fixed insolation and fixed SSTs so as to isolate this phenomenon in a simpler, statistically stationary framework.

The GCM employed is that developed by the Climate Dynamics Group at the GFDL. It has a global domain with realistic orography and land–sea contrast, with rhomboidal 30 truncation and 14 unequally spaced sigma levels. The physical packages in the model have been left unaltered. These include moist convective adjustment, gravity wave drag, a ground hydrology that includes formation of continental snow cover and a bucket for water storage, and a simple cloud prediction scheme dependent only on relative humidity. Climate statistics from a seasonal integration of this model have been documented by Alexander and Scott (1996) and are available at http://www.cdc.noaa.gov/gfdl/.

For our study, the model was forced with insolation, sea surface temperature, sea ice, and ozone concentrations that are fixed at values corresponding to the middle of each individual month. For each month from October to March, an integration of 1200 days was completed and the statistics of the last 1000 days are analyzed in this study.

Figure 1 depicts the rms of the bandpass filtered (2–6-day period) geopotential height field at 205 mb from the perpetual insolation model and Fig. 2 shows the time-mean zonal wind at the same level. Comparing the storm tracks in this model to those in observations, such as in Nakamura's (1992) analysis, we find that midwinter suppression is even more pronounced in this perpetual insolation GCM, with a reduction of 50% in variance in midwinter, as opposed to about 30% in observations. Comparison with the seasonal GCM referred to above (figures not shown) indicates that the perpetual model also has a stronger suppression than the more realistic seasonal model. Therefore, this perpetual insolation format evidently captures this phenomenon in a somewhat cleaner form.

In discussions of storm track structure based on geopotential variance, it is necessary to filter out low-fre-

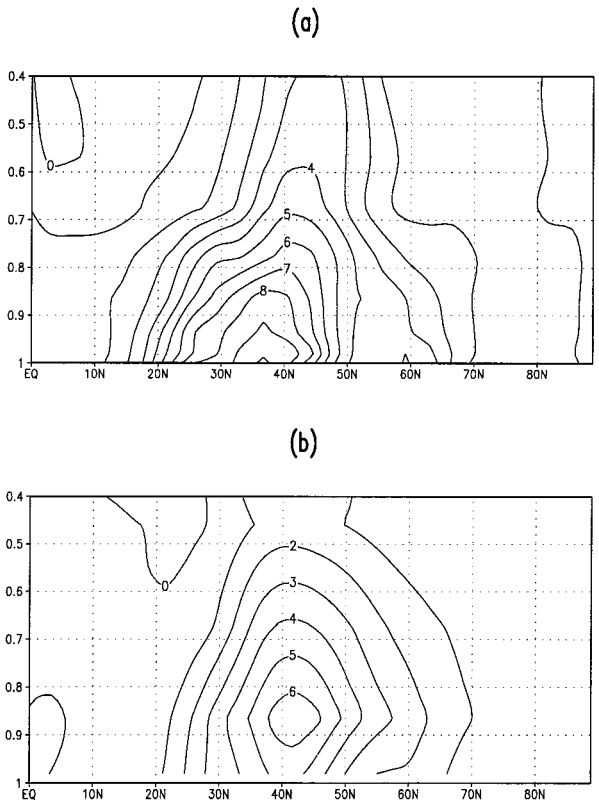

FIG. 4. The distribution of zonally averaged transient eddy heat fluxes from the linear stochastic model (a) and the R30 perpetual Jan GCM (b). Units: m s^{-1} K. Vertical axis: σ coordinates.

quency variability, as in Fig. 1 and in Nakamura (1992). The filtering is a potential source of confusion, as there could be shifts in the frequency of the eddies with season. With this in mind we have examined other measures of eddy activity that are more strongly dominated by high frequencies and do not require a filter to isolate the storm tracks. In particular, we find that the midwinter suppression is present in the meridional velocity variance field without filtering [see Zhang (1997) for these results]. We continue to use filtered geopotential here for easier comparison with previous work.

When we compare these GCM simulations with the observations, several differences are also apparent. The seasonal cycle as a whole is shifted about one month earlier since the heat capacity of the atmosphere creates roughly this much delay in the response to seasonally varying forcing. In Fig. 1, the maximum variance occurs in October and March, rather than in November and April as in observations. The seasonal cycle of the Atlantic storm track is not simulated well, as the observations have a better-defined maximum in midwinter. It is as if this perpetual model is on the verge of suppressing eddies in midwinter in the Atlantic as well.

Additional experiments in which we fix SST at their January value but allow the insolation to change show that the insolation change accounts for nearly all of this structure in the seasonal cycle. Because of the small changes of SST from, say, November to January this should not be surprising. We presume that the Pacific storm track is primarily responding to changing insolation over Eurasia.

Our goal is to determine if the storm track variation can be understood more directly as a response to changes in the time-mean flow. Having a theory for eddy fluxes given the mean flow, one could then hope to construct a theory for how the mean flow itself evolves due to the changing insolation.

3. Linear stochastic dry GCM

a. Constructing the model

Our starting point is the dynamic core of a 14-level primitive equation model with all forcing/dissipation terms removed. The model is discretized vertically in the same manner as the full GCM and is horizontally truncated at T30.

We start by linearizing this dynamical core around a certain climate generated by the GCM. Rayleigh friction and Newtonian cooling are then added to crudely model the boundary layer processes in the GCM. Letting $\mathbf{V}'$ and T' represent horizontal velocity and temperature perturbations, respectively, these damping terms have the form

$$\frac{d\mathbf{V}'}{dt} = \cdots - \alpha f(\sigma)\mathbf{V}' \tag{1}$$

$$\frac{dT'}{dt} = \cdots - \beta f(\sigma)T' \tag{2}$$

$$f(\sigma) = \begin{cases} \dfrac{\sigma - 0.7}{1.0 - 0.7}, & 0.7 \le \sigma \le 1.0 \\ 0, & \text{otherwise,} \end{cases} \tag{3}$$

where α represents boundary layer friction and β represents boundary layer thermal damping. Both are constants and their values are determined when the model is tuned. A biharmonic damping is also added to absorb the enstrophy of small scales. This damping coefficient is chosen such that the *e*-folding time for the smallest wave is 0.5 days, which is somewhat stronger damping than that used in the full GCM. There is no explicit topography in the model; however, it is implicitly present through the field of mean surface pressure. In this σ-coordinate model one can show that topography affects the linear dynamics only through its effect on the distribution of mean surface pressure. Finally, because our model uses σ as a vertical coordinate, the basic-state variables have steep gradients in the Tibetan Plateau region where the σ levels are strongly sloped. Small-scale numerical instabilities result from the steep gradient. While we do not understand them fully, we are able to eliminate these small-scale numerical instabilities by increasing the strength of the lower-level tem-

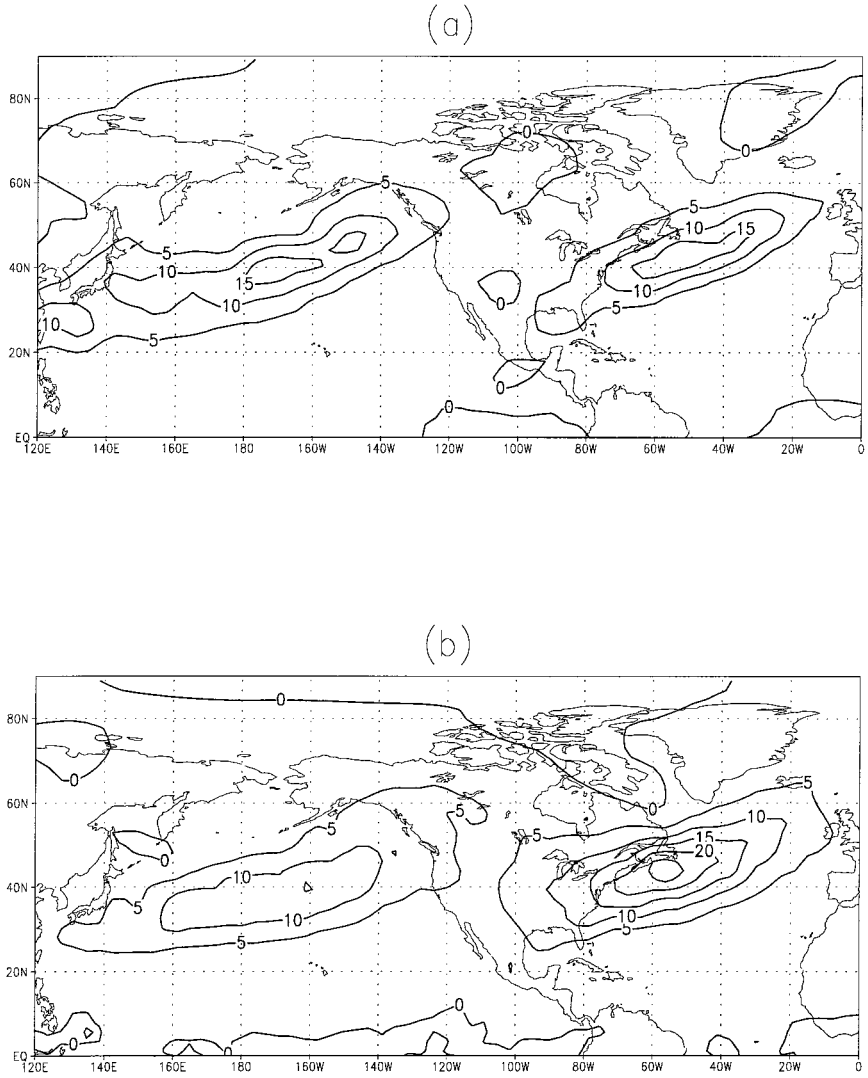

FIG. 5. The distribution of transient eddy heat fluxes at $\sigma = 0.865$ from the linear stochastic model (a) and the R30 perpetual Jan GCM (b). Units: m s^{-1} K.

perature and velocity damping in the region over the Tibetan Plateau. In this region the low-level damping coefficients α and β are both increased by a constant amount, 1.25 day^{-1}.

An overall uniform linear damping and white noise forcing are then added and the final linear stochastic model has the form

$$\frac{d\mathbf{X}}{dt} = (L - \gamma\mathbf{I})\mathbf{X} + \boldsymbol{\epsilon}. \tag{4}$$

Here $\mathbf{X}$ is the vector of all model variables, and L is the linear operator of the model including the dissipation and damping terms described above; $D = -\gamma\mathbf{I}$ is the additional linear damping meant to represent the nonlinear scrambling and $\mathbf{I}$ is the identity matrix. The forcing matrix $\boldsymbol{\epsilon}$ is white in time and in all three spatial coordinates, but even with this simplification one still has freedom in choosing the spatial structure of the variance of the noise and the relative strength of the forcing of different model variables. Although we have experimented with several alternatives, we focus here primarily on a model in which we include noise only in the lower troposphere ($\sigma > 0.76$) and between 20° and 60°N. We force only the temperature and vorticity equations.

Rather than try to obtain the eddy statistics by direct matrix inversion, given the large matrices involved we have chosen to integrate the stochastic model forward in time with the same semi-implicit time step as in the full GCM:

$$\frac{\mathbf{X}^{i+1} - \mathbf{X}^{i-1}}{2\delta t} = L_E\mathbf{X}^i + L_\mathbf{I}\left(\frac{\mathbf{X}^{i+1} + \mathbf{X}^{i-1}}{2}\right) - \gamma\mathbf{X}^{i-1} + \boldsymbol{\epsilon}^i. \tag{5}$$

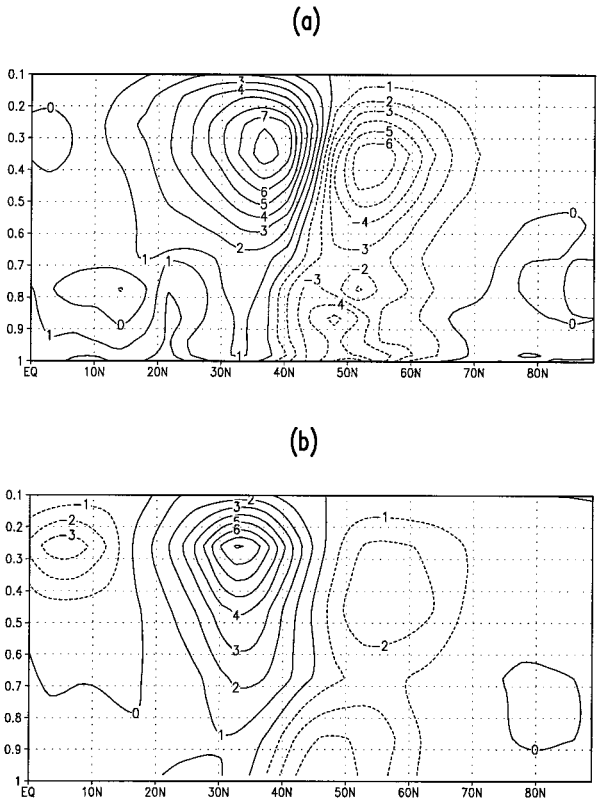

FIG. 6. The distribution of zonally averaged transient eddy momentum fluxes for the linear stochastic model (a) and the R30 perpetual Jan GCM (b). Units: $m^2\ s^{-2}$. Vertical axis: σ coordinates.

Here L_E and L_I represent the terms treated explicitly and implicitly, respectively. A time filter is used each time step to relax $\mathbf{X}^i$ to the mean of $\mathbf{X}^{i+1} + \mathbf{X}^{i-1}$, just as in the GCM. The noise is given by $\epsilon = \epsilon_0 R$, where R is a random number having a Gaussin distribution with unit variance and ϵ_0 is a constant if δt is modified, the noise should be multiplied by $(\delta t)^{-1/2}$ to maintain the same variance, assuming that δt is shorter than any dynamically relevant timescales. The time step δt is 1728 s (50 steps per day) in all of our experiments. The strengths of the forcing in the temperature and vorticity equations are denoted by $\epsilon_0 = \epsilon_T$ and $\epsilon_0 = \epsilon_V$, respectively. The same values are used at all points in the horizontal and vertical at which the forcing is not set explicitly to zero.

b. Tuning the model

Our model has been explicitly tuned; that is, the parameters α, β, γ, and (ϵ_T, ϵ_V) were adjusted until various second-moment statistics produced by the model match those generated by the original nonlinear GCM when its time-mean flow serves as the linear model's basic state. In this tuning process, we choose the perpetual January GCM as the target nonlinear system. Accordingly, the basic state of the linear stochastic model is the 1000-day-averaged climate of the perpetual January GCM. The linear model is run for 500 days and the last 400 days are used to construct the eddy statistics.

Although we have not systematically searched the entire parameter space, we have found a reasonably good fit to the geopotential variance and poleward eddy heat and momentum fluxes with $\alpha = 0.83\ \text{day}^{-1}$, $\beta = 1.67\ \text{day}^{-1}$, $\gamma = 0.063\ \text{day}^{-1}$, $\epsilon_V = 8.1 \times 10^{-11}\ \text{s}^{-2}$, and $\epsilon_T = 4.1 \times 10^{-6}\ \text{K s}^{-1}$. The sensitivity of the model-produced second-moment statistics to these parameters will be discussed later in the paper.

Figure 3 shows the storm tracks at 350 mb from the perpetual January GCM and from the linear model. Since the linear stochastic model is meant to model the high-frequency eddies in the perpetual GCM, the nonlinear time series are bandpass filtered when the eddy statistics are calculated. When tuned in this way, the stochastic model provides relatively little low-frequency variability and requires no time filter. The linear model performs very well in simulating the two oceanic storm tracks. The position and relative magnitude of the Pacific and the Atlantic storm tracks and the northeastward tilt of the Atlantic storm track are all captured by this linear model.

Eddy heat and momentum fluxes are of central importance in the maintenance of climate and its low-frequency anomalies. How well the linear model can reproduce these flux terms will serve as an important indicator of the model's performance. It is found that with this set of parameters the eddy heat and momentum fluxes are also reproduced quite well. As in the calculation of geopotential height variances, the GCM eddy fields have been bandpass (2–6 day) filtered to retain the information on baroclinic eddies.

Figure 4 depicts the vertical structure of the zonally averaged heat flux from the linear model and the perpetual January GCM. We see that in both models the maximum heat flux is located near 40°N and the vertical axis of the flux tilts slightly poleward. In the linear model, the heat flux is trapped closer to the surface than in the perpetual January GCM. In Fig. 5 we show the horizontal structure of eddy heat flux at $\sigma = 0.865$. It can be seen that the overall distribution and the magnitude of heat fluxes in the Pacific storm track are produced very well by the linear model, though the heat flux in the Atlantic storm track is somewhat smaller than that in the GCM. We return to this point in section 3d.

In Fig. 6 we show the zonally averaged meridional momentum flux $\overline{u'v'}$ from the linear model (Fig. 6a) and the perpetual January GCM (Fig. 6b). We see that in the GCM, most of the momentum fluxes are concentrated near the tropopause. The dominant feature is the strong northward momentum flux around 30°N flanked by two regions where the momentum is transported southward. Another region of southward momentum transport can be observed around 50°N at the surface levels. The overall distribution and the strong northward momentum flux around 30°N are captured by

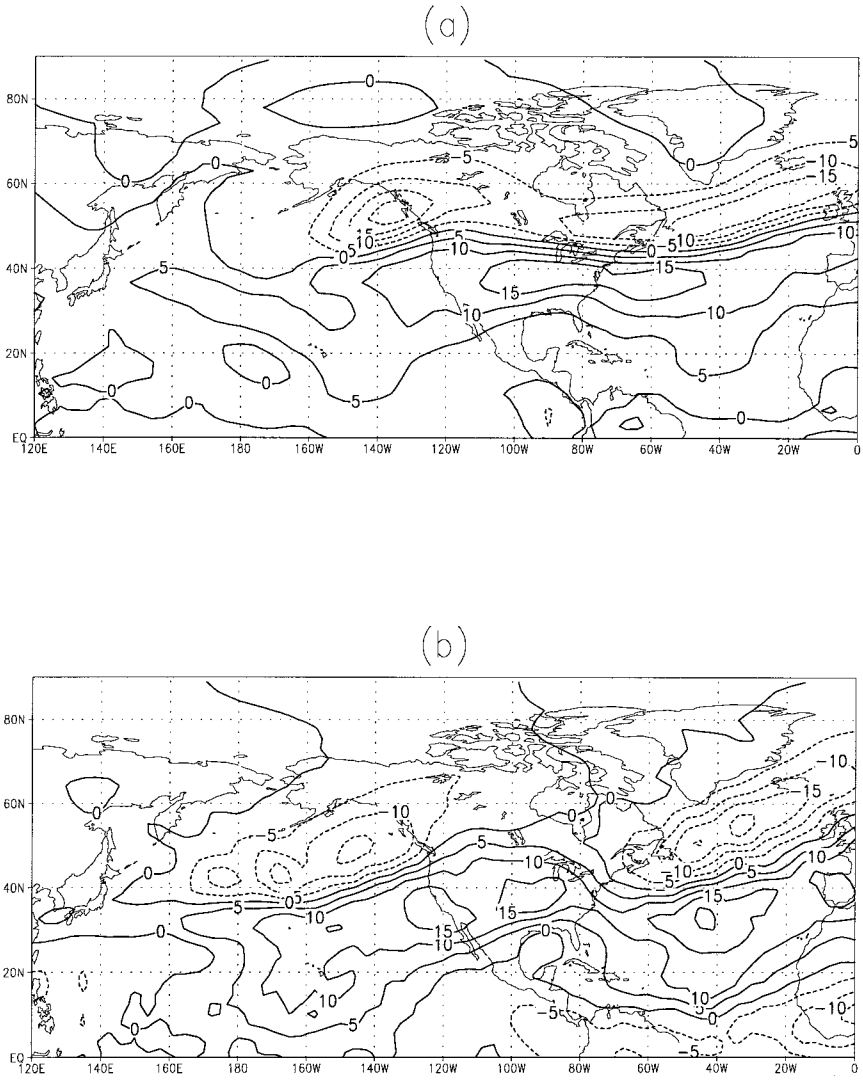

FIG. 7. The distribution of transient eddy momentum fluxes at $\sigma = 0.26$ for the linear stochastic model (a) and the R30 perpetual Jan GCM (b). Units: $m^2\ s^{-2}$.

the linear model fairly well, though the weak southward momentum transport around 50°N is overestimated by the linear model.

Figure 7 depicts the meridional momentum flux at $\sigma = 0.26$ for the two models. The pattern of the momentum flux is not as well simulated as the pattern of the heat flux. The momentum fluxes are shifted eastward somewhat in the Pacific as compared with the GCM. The fluxes are also too zonally symmetric in the Atlantic.

c. The propagation of eddies in the linear model

Lag-correlation maps of bandpass filtered data are useful for illustrating the statistical structure and evolution of high-frequency disturbances (Wallace et al. 1988). Since the linear model has been designed to simulate the baroclinic eddies in the GCM, unfiltered data are used to calculate the lag-covariances. Data from the nonlinear GCM are still bandpass filtered as above.

Figures 8 and 9 show the lag-correlation maps of the geopotential height at 350 mb from the GCM and the linear model for lags −2, 0, +2 days. The reference point is located at (40°N, 180°). Although wave propagation is clearly present in the linear model, the wave train is not as persistent and part of the Pacific wave train is refracted too strongly into the Tropics. This result is improved slightly when a bandpass filter is applied to the data from the stochastic model as well (not shown)

To further study the wave propagation properties in the linear model we have conducted experiments in which we force the temperature and vorticity equation separately. These experiments indicate that temperature

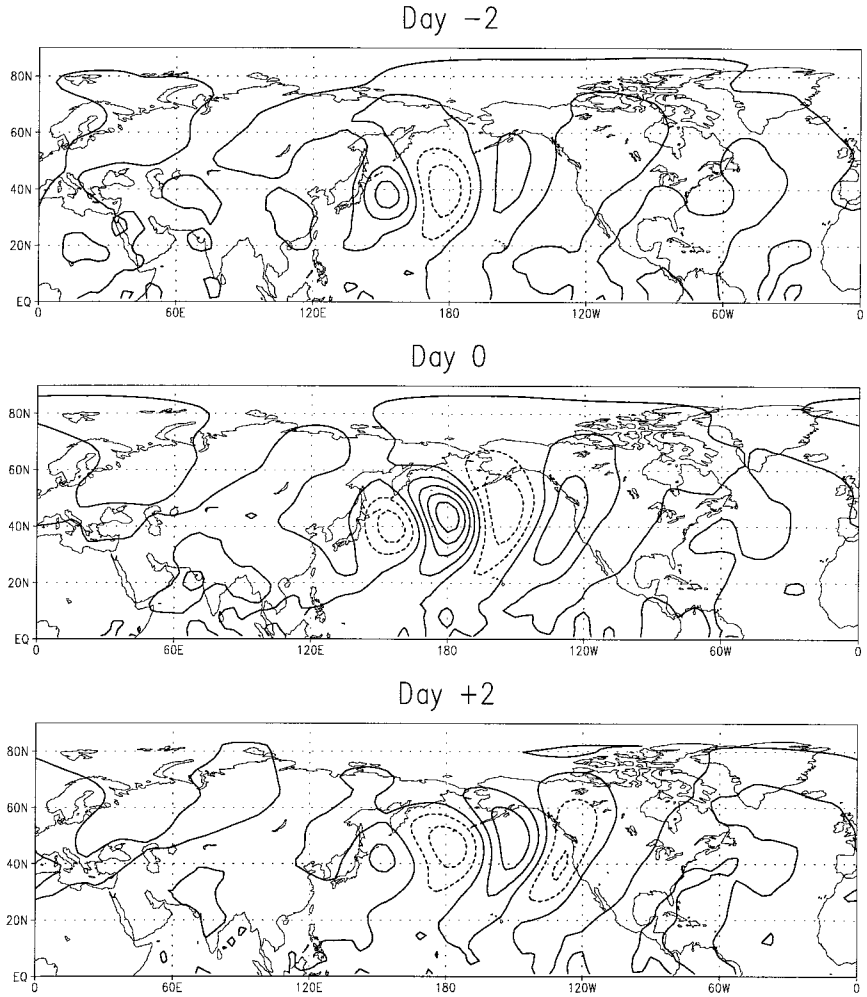

FIG. 8. One-point correlations of bandpass filtered geopotential height at 350 mb from the R30 perpetual Jan GCM. Reference point is (40°N, 180°).

forcing produces a more persistent, zonally propagating wave train and vorticity forcing is more responsible for the propagation to the Tropics. This difference appears to be a consequence of the fact that white noise temperature forcing excites smaller horizontal scales than white vorticity forcing, and these smaller scales do not propagate as efficiently into the Tropics. We have experimented with the model parameters to determine how best to mimic the GCM's wave train. In Fig. 10 we perturb the temperature equation everywhere over the globe, at all levels, with noise that is once again white in the vertical as well as in the horizontal. In this case, the stochastic model produces significant low-frequency variability, so a bandpass filter is applied to the 350-mb geopotential height. Under these conditions the model produces a wave train that resembles fairly closely that in the GCM, but the fluxes generated by this model are less satisfactory than those shown earlier in this section. Within our self-imposed constraints of spatial white noise forcing vorticity and temperature, we have not found parameters for which the dominant wave train and the eddy fluxes of heat and momentum are all well-simulated simultaneously.

d. Sensitivity studies

Our primary goal in tuning the model was to reproduce the second-moment statistics of the perpetual GCM. In particular, we have concentrated on the horizontal and vertical distribution of geopotential height variance, heat fluxes, and momentum fluxes. In this section we show how these characteristics change when the model parameters deviate from the control values described above. When a parameter is changed in the experiments described in this section, we always readjust the strength of the stirring so that the magnitude of the geopotential height variance at the center of the Pacific storm track at 350 mb matches that in the GCM. This is equivalent to examining the relative magnitudes of the fluxes and variances relative to the 350-mb geo-

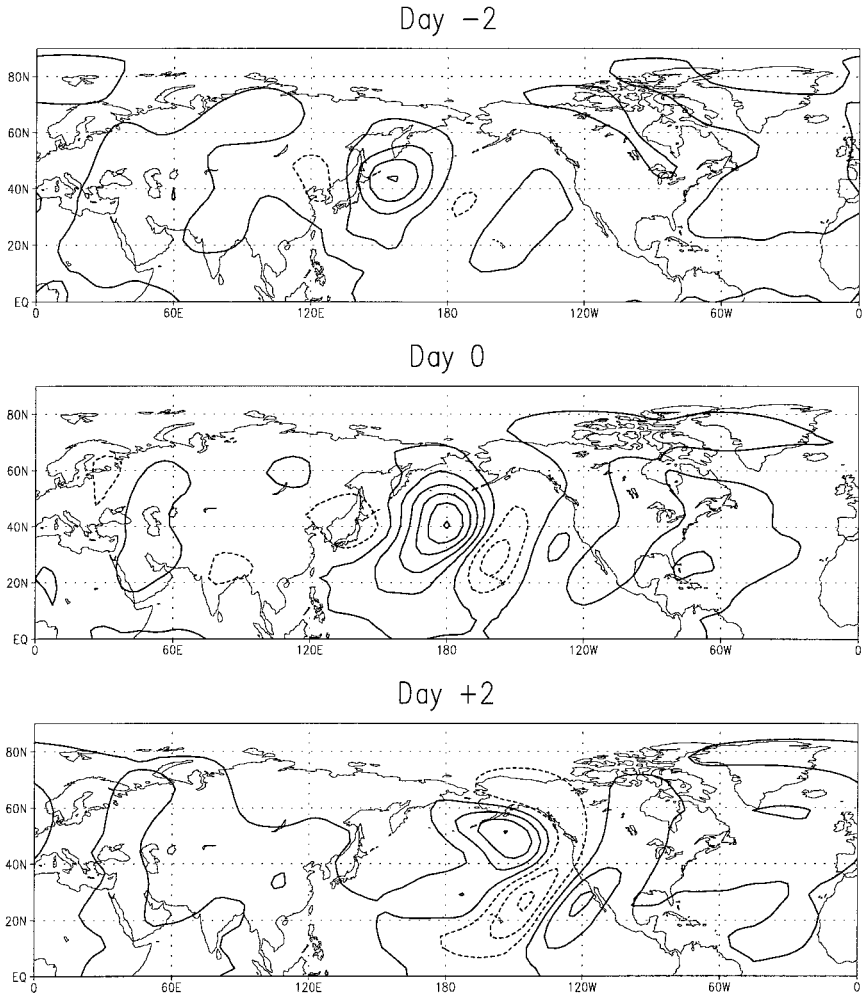

FIG. 9. One-point correlations of geopotential height at 350 mb from the linear stochastic model. Reference point is (40°N, 180°).

potential height variance at the center of the Pacific storm track.

We first examine the model sensitivity to the lower-level mechanical damping and Newtonian cooling. We find that the lower-level heat flux is most sensitive to the change of these parameters. Figure 11 shows the heat flux at $\sigma = 0.865$ with $\alpha = 0.42$ (a), 0.83 (b), and 1.25 (c) day^{-1} [the results described above correspond to (b)]. The strength of the stirring ϵ_V, ϵ_T is adjusted to (5.5×10^{-11} s^{-2}, 2.8×10^{-6} K s^{-1}) in (a) and (1.0×10^{-10} s^{-2}, 5.2×10^{-6} K s^{-1}) in (c). (The ratio of ϵ_V to ϵ_T is held fixed in this readjustment.) All the other parameters are kept the same as in (b). When the lower-level mechanical damping is weakened (decreasing the strength of the stirring to keep the upper-tropospheric geopotential variances in the Pacific at the right level), it is primarily the heat flux in the Atlantic storm track that increases.

The model responds differently to a change in the Newtonian cooling. In Fig. 12a we reduce β to 0.83 day^{-1} and ϵ_V, ϵ_T to (6.1×10^{-11} s^{-2}, 3.0×10^{-6} K s^{-1}). The heat flux is doubled in both storm tracks. We can no longer simultaneously generate the correct magnitude of the upper-level eddy variance and the low-level heat flux. When β is increased to 2.5 day^{-1} and ϵ_V, ϵ_T to (9.4×10^{-11} s^{-2}, 4.7×10^{-6} K s^{-1}) in (c), the heat flux consistently decreases in both oceans. The relative magnitude of the heat fluxes over the two oceans does not change appreciably. In short, while mechanical damping and Newtonian cooling both affect the strength of the lower-level heat fluxes in the storm tracks, for fixed upper-level eddy amplitudes in the Pacific, the mechanical damping can further control the relative magnitudes of the heat fluxes in the two oceanic storm tracks. The upper-level momentum fluxes are not very sensitive to these two parameters in the range we have covered, given that we adjust the stirring level in each case to maintain the same upper-troposphere variances. Though

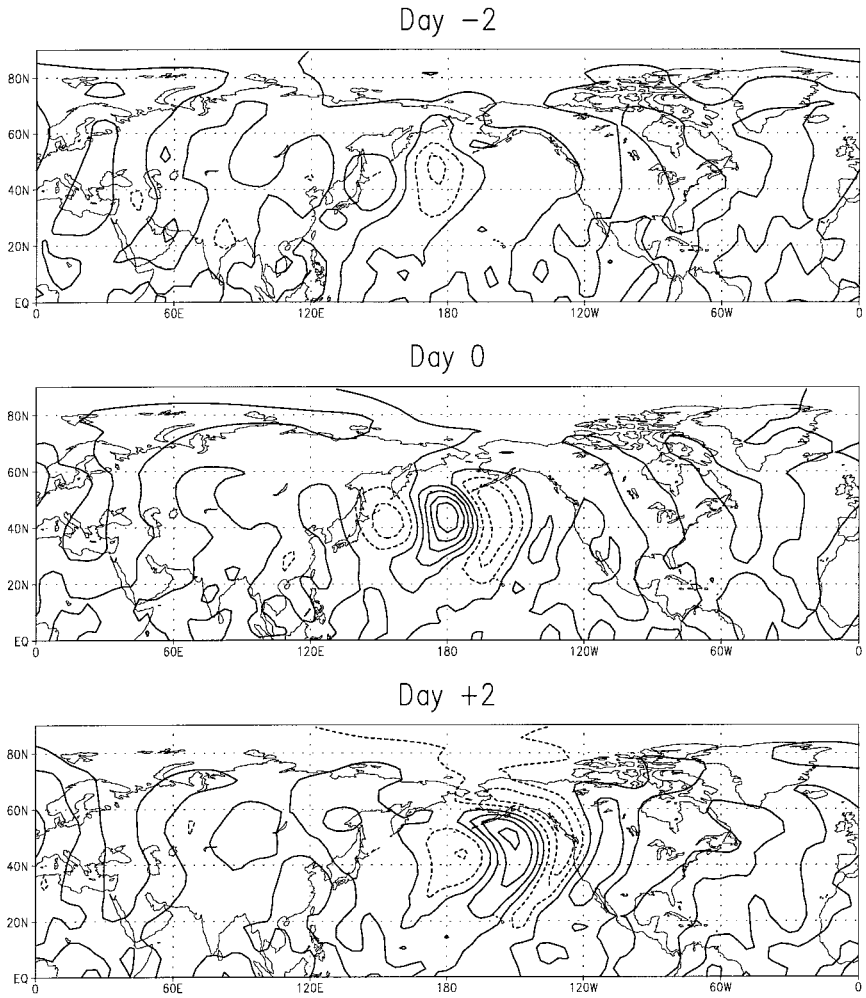

FIG. 10. One-point correlations of geopotential height at 350 mb from the linear stochastic model when only the temperature equation is forced everywhere. Reference point is (40°N, 180°).

stronger damping naturally brings weakened lower-level eddy statistics, the vertical profiles of fluxes and variances do not change drastically in these experiments.

We have also examined aspects of the model sensitivity to the horizontal distribution of the random forcing, continuing to assume that it is spatially uncorrelated. In one experiment, shown in Fig. 13, we perturb the temperature and vorticity field between 20° and 60°N and below $\sigma = 0.76$, just as in our standard case, but only in a longitudinally confined region over Asia between 30° and 90°E. The other parameters assume the same values as in the standard integration. Compared to the standard run in which temperature and vorticity are forced everywhere in the extratropics, this experiment produces a well-defined Pacific storm track, while the Atlantic storm track is very weak. Since part of the Pacific wave train is strongly refracted into the Tropics in this version of the stochastic model, the Atlantic storm track is not seeded very efficiently by eddies coming from the Pacific, and therefore the Atlantic storm track is hardly present when only a local region upstream of the Pacific Ocean is perturbed.

It is interesting to compare this result with that in which we perturb only the temperature equation between 20° and 60°N, 30° and 90°E but at all levels in the vertical, shown in Fig. 14. We expect a persistent wave train propagating more directly from the Pacific to the Atlantic Ocean in this version of the model, as already seen in Fig. 10. Consistently, this version produces a well-defined Atlantic storm track, even without stirring in the Atlantic sector. It is interesting that this kind of change in the structure of the stirring can have such a dramatic impact on the upstream seeding of the storm tracks.

To explore this sensitivity further we have repeated this experiment with several other distributions of forcing, including vorticity forcing at all levels, vorticity forcing at low levels only, and temperature forcing at low levels only. In all cases, the forcing is once again localized in the same central Asian region. It is found

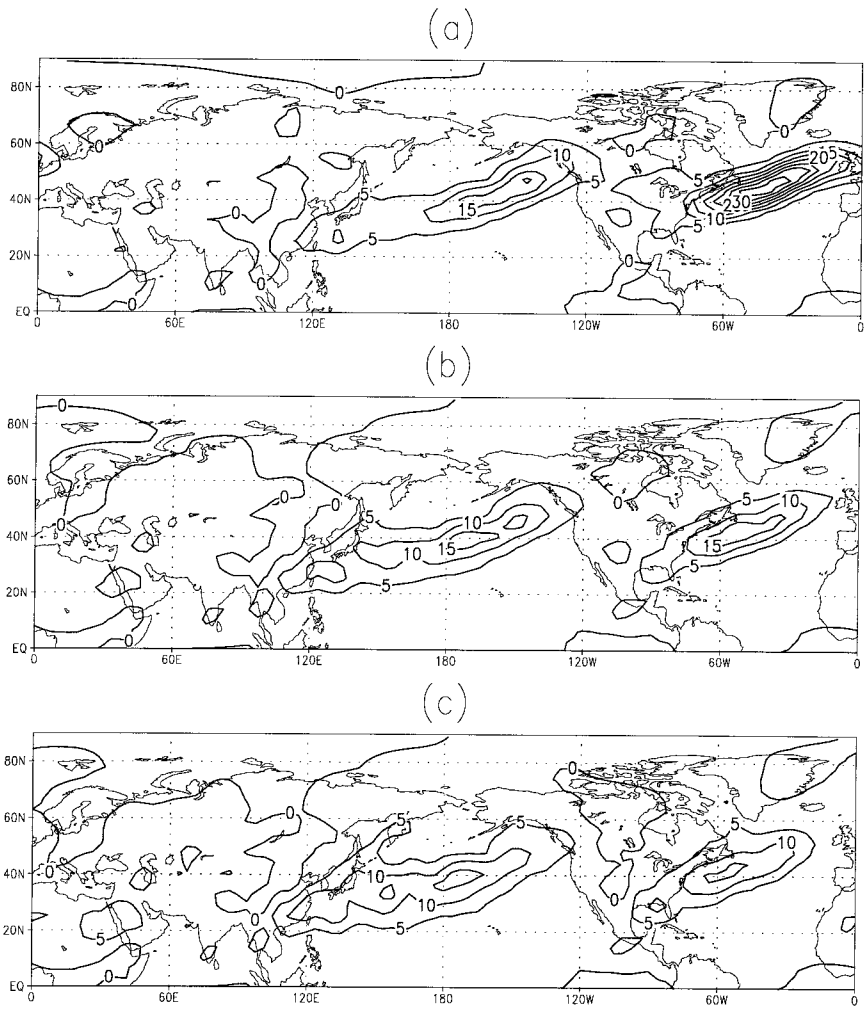

FIG. 11. The distribution of transient eddy heat fluxes at $\sigma = 0.865$ from the linear stochastic model: $\alpha =$ (a) 0.42, (b) 0.83, and (c) 1.25 day^{-1}. Units: m s^{-1} K.

that temperature forcing produces a stronger Atlantic storm track, for a given strength of the Pacific storm track, than vorticity forcing with the same vertical structure. Further, perturbing at all vertical levels rather than only at low levels also generates a stronger Atlantic storm track.

We do not understand these results fully. When fitting the variances and fluxes, we find it to be beneficial to localize the stirring at low levels. Conservation of wave action causes eddy energy and geopotential variance to increase as eddies propagate upward into a region of stronger westerlies, a fact of central importance to the structure of the singular vectors that define those structures which can grow most rapidly over finite time intervals (see Buizza and Palmer 1995). The larger scales propagate upward more easily and these larger scales appear to be needed to obtain the correct amplitudes for the upper-tropospheric eddy fluxes. If one forces only at upper levels, the solution is noisier, less dominated by particular waves that have been selectively amplified. But in fitting the structure of the Pacific wave train and its ability to seed the Atlantic, the inclusion of some upper-tropospheric stirring is useful in creating disturbances that propagate more zonally. As stated earlier, spatially white temperature forcing, as contrasted with spatially white vorticity forcing, also seems to favor smaller scales that do not radiate as strongly into the Tropics and therefore propagate more easily from the Pacific into the Atlantic.

The overall damping γ also has an effect on the relative magnitudes of the two storm tracks, but this sensitivity is itself sensitive to the structure of the forcing. When γ is increased in our control linear model, with stirring only at low levels, the Atlantic storm track gets somewhat weaker with respect to the Pacific storm track, but this change is not very large. (We do not display this result here.) This is consistent with the picture that a large part of the Pacific wave train is refracted into the Tropics instead of propagating into the Atlantic Ocean so that γ cannot easily regulate the relative

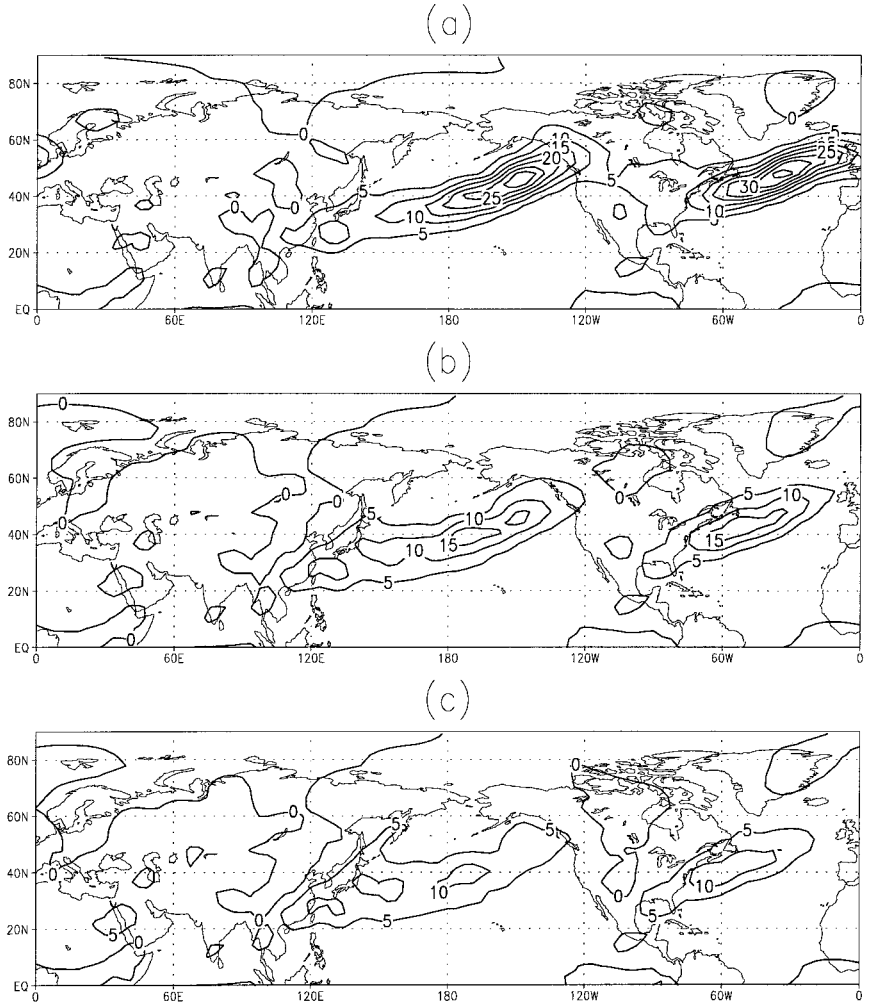

FIG. 12. The distribution of transient eddy heat fluxes at $\sigma = 0.865$ from the linear stochastic model: $\beta =$ (a) 0.83, (b) 1.67, and (c) 2.5 day^{-1}. Units: m s^{-1} K.

strength of the two storm tracks. In the case where only temperature forcing is present at all levels and the wave train tends to propagate more directly into the Atlantic Ocean, the relative magnitude of the two storm tracks is more sensitive to the change of γ, as shown in Fig. 15, with weaker γ producing a relatively strong Atlantic storm track.

4. Seasonal and interannual variation of storm tracks in the linear stochastic model

In the previous sections we have shown that the stochastic model is capable of reproducing many features of the climatological storm tracks of the perpetual January GCM, such as the horizontal and vertical distribution of variances and momentum and heat fluxes. We have also shown that these eddy statistics are sensitive to the lower-level boundary layer dampings. The power of a stochastic model of this kind will be determined by its ability to predict storm track variations without retuning the model when the basic state is altered. In this section we examine the sensitivity of the storm tracks to the basic-state changes associated with seasonal and interannual variations.

a. The midwinter suppression of the Pacific storm track in the linear stochastic model

Having tuned the linear model with the perpetual January data, we now change the basic state of the linear model to the time-mean flow of the other five perpetual runs without changing any other model parameters. All the procedures to run the stochastic model and to obtain the statistics are unaltered. All parameters in the linear model are kept fixed, including the amplitude of the white noise forcing. Figure 16 shows the rms of geopotential height at 205 mb obtained from the linear model using the six time-mean flows as the basic state. Comparing these figures with their counterparts from the perpetual GCM runs in Fig. 1, we see that the seasonal

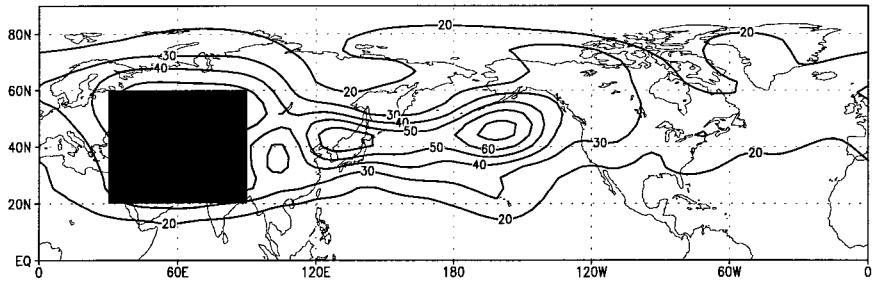

FIG. 13. The distribution of rms of the geopotential height at 350 mb produced by the linear stochastic model when only the region between 20° and 60°N, 30° and 90°E is perturbed (vorticity and temperature forcing at low levels). Units are meters.

variation of the intensity of the Pacific storm track is largely captured by the linear model. Most interestingly, the midwinter suppression of the Pacific storm track is qualitatively produced by the linear model, though the degree of suppression is less than in the nonlinear model, and one of the two maxima is found in November instead of in October. Significant differences are found in February, with the relative strength of the Atlantic and Pacific storm tracks poorly reproduced in the linear model. The linear model also captures the eastward shift of the Pacific storm track from fall to midwinter. The result is robust with respect to changes in model parameters. In particular, when the model is tuned to obtain a more zonally propagating wave train (Fig. 10), this predicted seasonal cycle is qualitatively unchanged.

b. Modeling the interannual variation of storm tracks during El Niño episodes

Having shown that the model does fairly well in simulating the seasonal variation of the storm tracks, we now check if it is able to capture the basic features of storm track variations associated with ENSO.

The ''control climate'' we choose for this purpose is the 30-yr-mean DJF (Dec–Feb) from a GFDL 14-level seasonal R30 GCM. The ''control storm track'' is also defined during this DJF period and averaged for 30 years. The ''ENSO climate'' is the average of four integrations for the 1982/83 DJF from a series of ENSO experiments carried out by the GFDL's Climate Diagnostics Group. The ''ENSO storm track'' is first calculated for each 1982/83 DJF period and then averaged over four integrations.

In Fig. 17 we present the rms of the bandpass filtered DJF geopotential height at 205 mb for the control storm track (a) and the ENSO storm track (b). The difference between (b) and (a) is shown in (c). We see that in the winter of the El Niño years, while the Atlantic storm track shifts southeastward, the Pacific storm track shifts southward, with a modest intensity increase in the model. In Fig. 18 (M. Ting 1998, personal communication) we show the regression of monthly mean bandpass transient eddy kinetic energy against the El Niño index for the period from November through March of 1979–94 using NCEP/NCAR twice-daily reanalysis wind data. The El Niño index used for this purpose is the time series of the first EOF of Pacific SST. This ENSO composite is not quantitatively comparable to the GCM simulations of 1982/83, but it illustrates that the GCM responds in a fairly realistic way to the imposition of ENSO boundary conditions, especially over the Pacific.

Figure 19 depicts the control storm track (a), the ENSO storm track (b), and the difference between the two reproduced by the linear stochastic model. Comparing Fig. 19a with Fig. 17a, we see that the overall distribution of the two storm tracks in the El Niño winters are reproduced yet the magnitude is somewhat underestimated. The southward shift of the storm tracks in the El Niño winters is captured fairly well by the

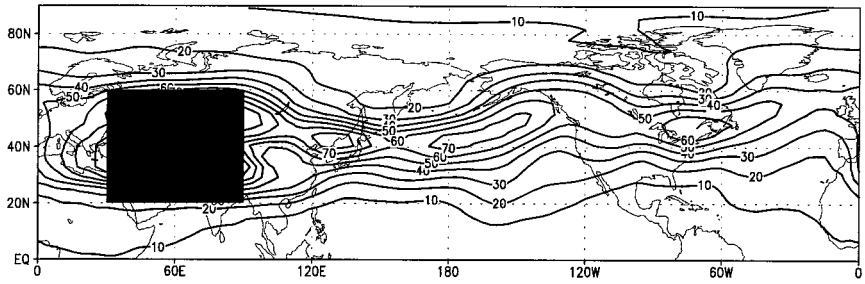

FIG. 14. The distribution of rms of the geopotential height at 350 mb produced by the linear stochastic model when only the region between 20° and 60°N, 30° and 90°E is perturbed (temperature forcing only, at all levels). Units are meters.

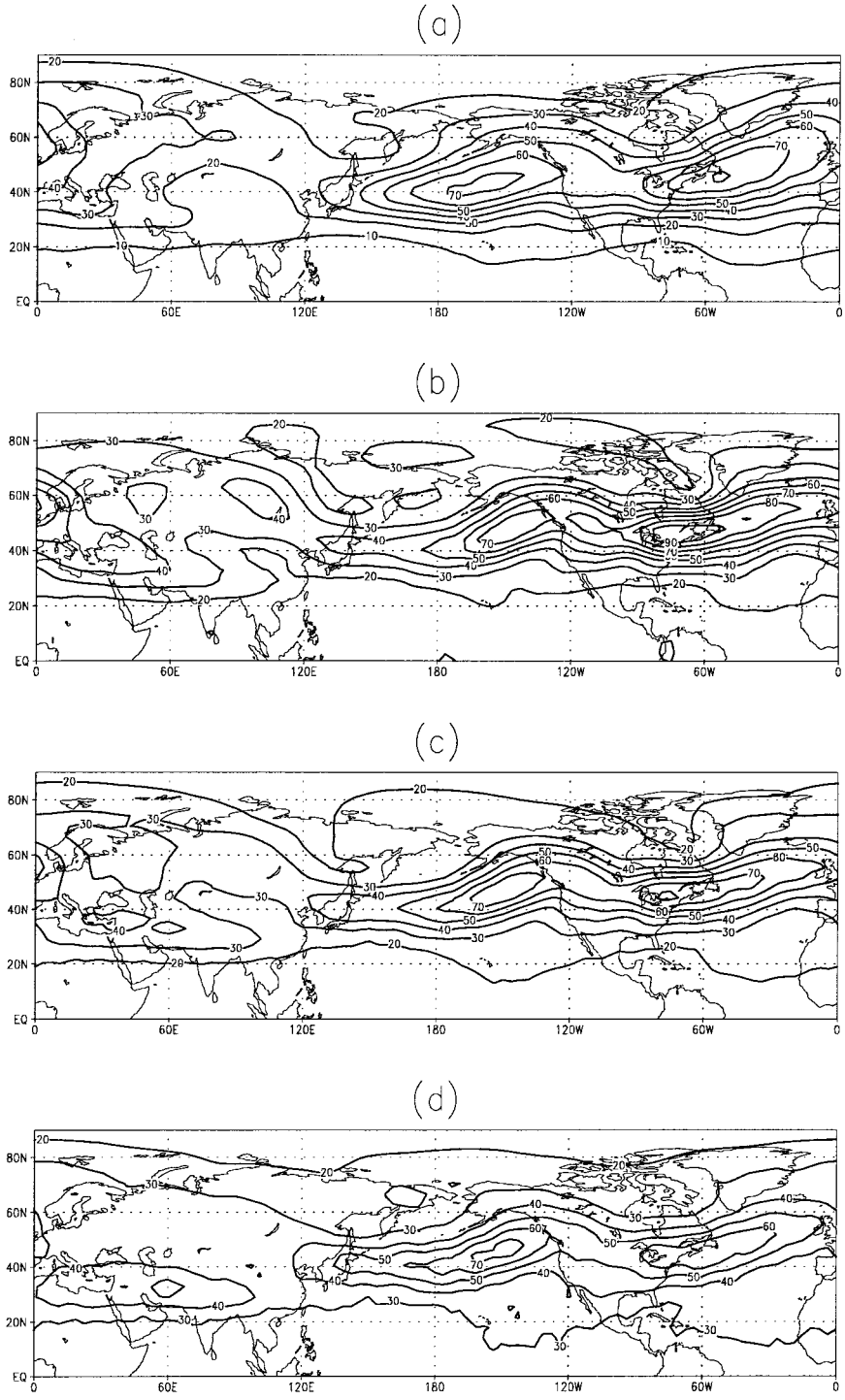

FIG. 15. The horizontal structures of the rms of the geopotential height at 350 mb from the perpetual Jan run (a) and from the linear model when temperature fields at all levels are perturbed and γ = (b) 0.083, (c) and 0.125, and (d) 0.25 day^{-1}. Units are meters.

linear model. However, the modest strengthening of the Pacific storm track during ENSO is not present in the linear model. In fact, the model predicts a slight weakening of the stormtrack.

5. Conclusions and discussion

The goal of this work is to relate the nonlinear baroclinic eddy statistics to the climatological mean flow.

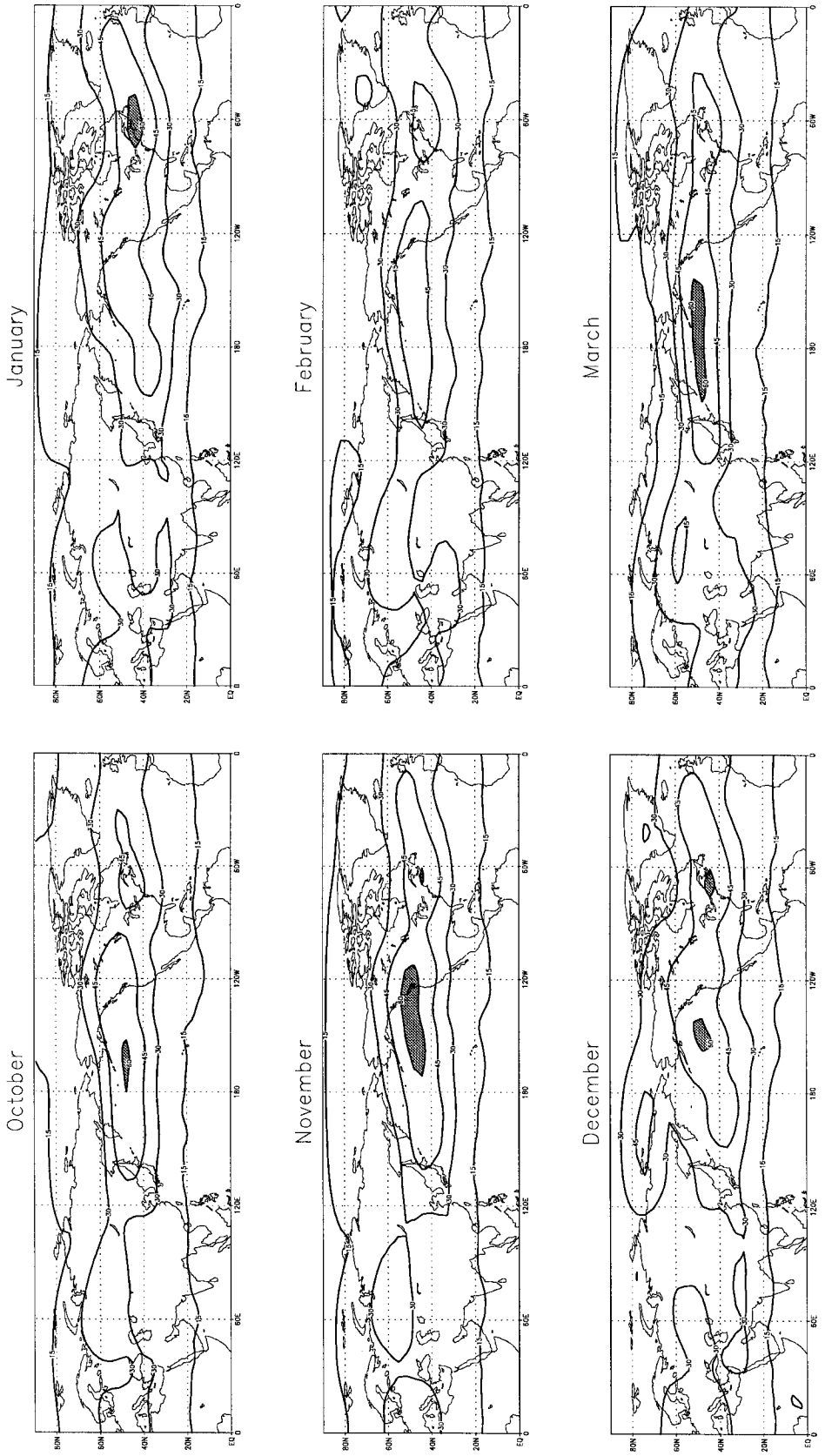

FIG. 16. The distribution of rms of the geopotential height at 205 mb produced by the linear stochastic model. Units are meters.

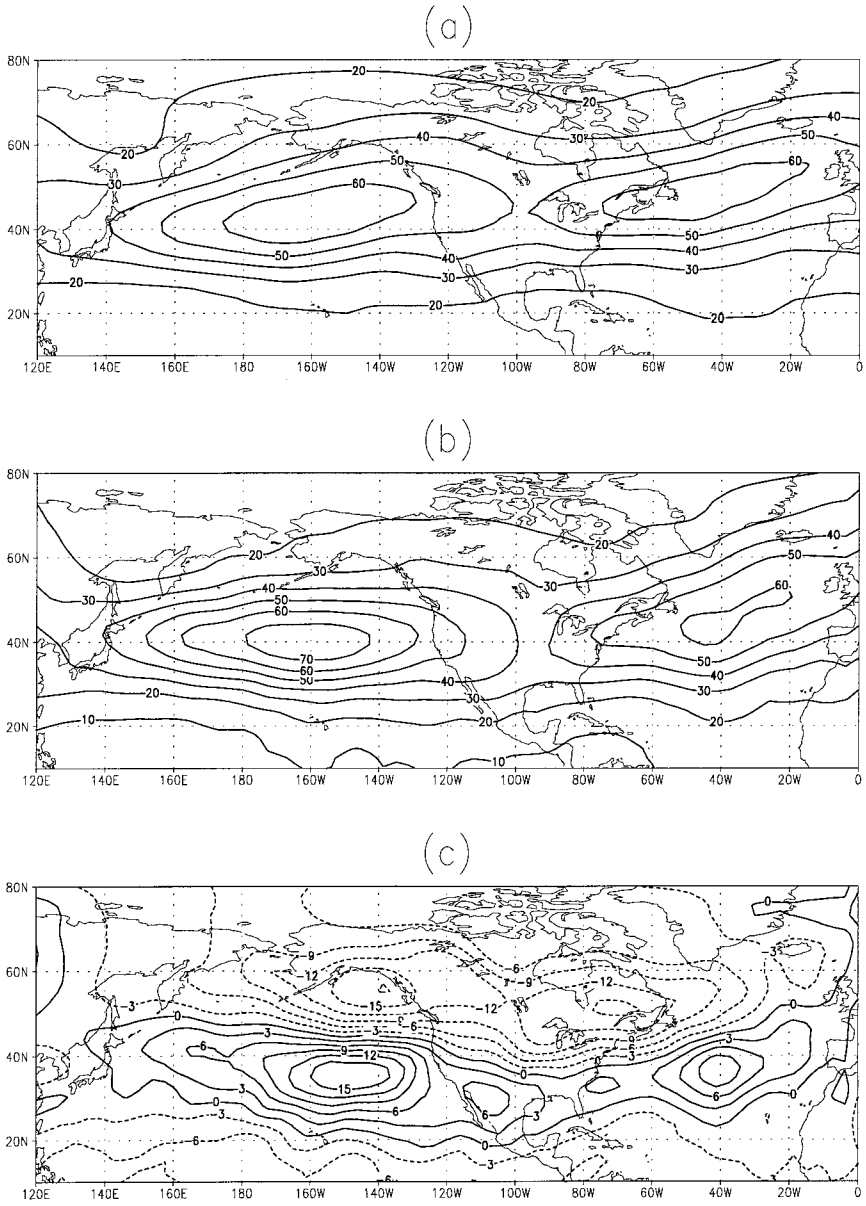

FIG. 17. The rms of the bandpass-filtered geopotential height at 205 mb during DJF: (a) from the 14-level seasonal GCM, (b) from the 1982/83 ENSO experiment, and (c) the difference between (b) and (a). Units are meters.

We have first constructed a linear stochastic model by adding linear damping and white noise forcing terms to a linearized primitive equation model. With the parameters chosen appropriately, the linear stochastic model can reproduce with a fair degree of accuracy the eddy geopotential variance as well as eddy heat and momentum fluxes of the perpetual January GCM, when the perpetual January climate is used as the linear model's basic state. Constraining our subjective tuning to spatially white forcing, the best result is obtained using forcing in both the temperature and vorticity that is localized in the lower troposphere. However, when tuned in this way, the Pacific wave train is refracted too strongly into the Tropics. If we try to correct this deficiency by stirring at upper levels, as well as by forcing the temperature equation preferentially, which produces a more zonally elongated wave train, we lose fidelity in our simulation of the fluxes.

The modeled heat fluxes are sensitive to the lower-level friction and Newtonian cooling coefficients, while the momentum fluxes respond only weakly to these changes in low-level damping if the stirring is adjusted to maintain the correct upper-level eddy variance in the Pacific storm track.

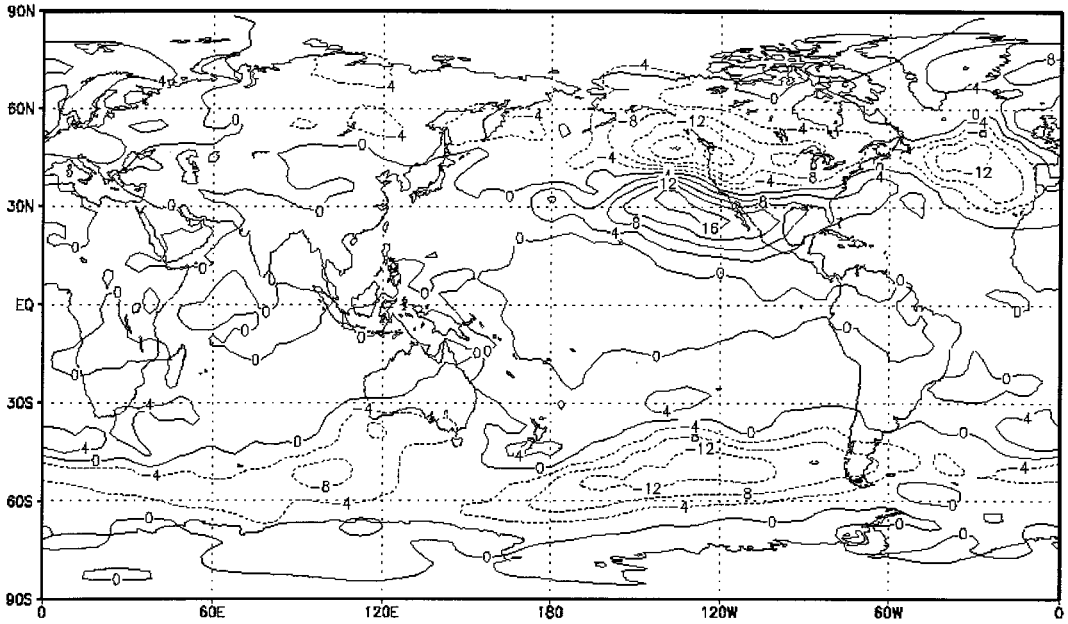

FIG. 18. Regression map of monthly mean bandpass transient eddy kinetic energy against the El Niño index based on the data during the period Nov through Mar of 1979–94. The original wind data were taken from NCEP–NCAR twice-daily reanalysis. The El Niño index is the time series of the first EOF of Pacific SST.

To examine the model's predictive power we predict the storm track seasonal variation from the seasonal changes of the time-mean flow. This effort has been generally encouraging. The seasonal change of the Pacific storm track intensity and its location are reproduced to a certain degree by the linear stochastic model. The midwinter suppression is present qualitatively, but the suppression is weaker than in the GCM. Since the amplitude of the eddy stirring should increase as eddy amplitudes increase, models with fixed stirring potentially miss a positive feedback from changes in stirring amplitude. So we should not be surprised by the muted character of the linear model's suppression.

This result suggests that the midwinter suppression can be attributed at least partly to the variation in structure of the background flow, as one progresses through the winter season. One should now be able to analyze the linear model dynamics to establish a better theoretical understanding of the phenomenon. We can immediately deduce from this result that the direct effects of latent heat release on the eddies is not of dominant importance in this seasonal cycle, for our linear model does not include any effects of moisture on the eddies. However, we cannot totally exclude the possibility that latent heating effects enhance the suppression somewhat.

As for interannual variations, the model has the capacity to reproduce the shift of storm tracks associated with ENSO, although the change of storm track magnitude is not captured with a fixed level of stirring. Once again, we should not expect to be able to explain changes in eddy amplitudes quantitatively with fixed stirring amplitudes.

It is interesting that we are able to produce realistic heat fluxes and momentum fluxes simultaneously, in contrast to the related study of Whitaker and Sardeshmukh (1997) using a two-layer model. The freedom we have given ourselves in perturbing both the temperature and vorticity field when tuning the model could account for this improved result. If we think of the forcing of potential vorticity, modifying the ratio of the vorticity to the temperature forcing is, in part, a crude way of modifying the spatial spectrum of the most dynamically relevant part of the forcing. On the other hand, it may be that we are not obtaining these flux patterns for entirely correct reasons, since the shape of the model's dominant wave trains in the Pacific is distorted.

While this stochastic approach is promising, we clearly need theoretical guidance on how best to stir and to damp the linear model. The stirring and damping must eventually be tied to the eddy statistics themselves, as in turbulent closure theories.

Rather than linearizing about the time-mean flow, assuming a form for the damping, and then tuning the damping parameters, one can also try to optimize the fit of the stochastic model to the GCM or observations more directly, as described by DelSole (1996) in his two layer quasigeostrophic experiments. One should be able to fit the eddy statistics more accurately with this approach since the choice of the time-mean flow as the flow about which to linearize and the choice of the form of the damping are both somewhat arbitrary. The dis-

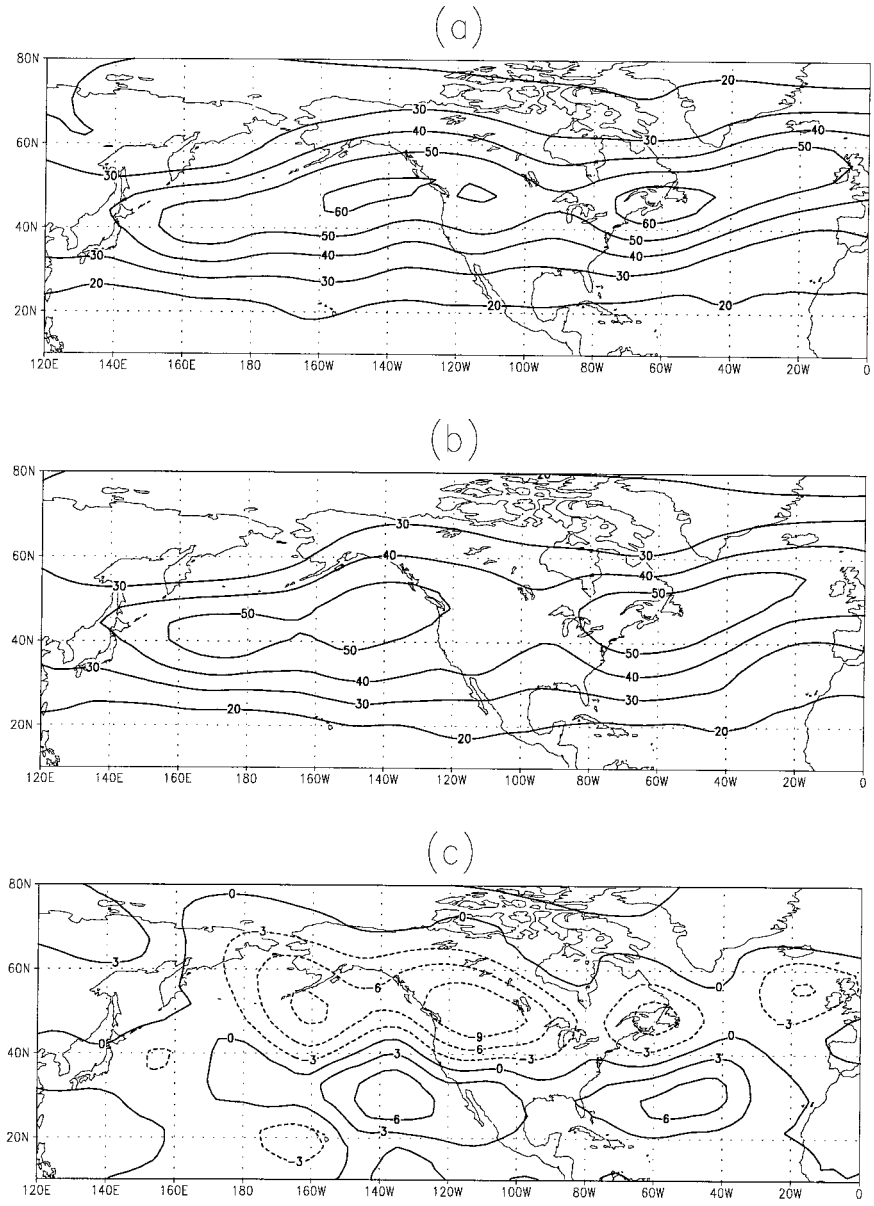

FIG. 19. The rms of the geopotential height at 205 mb from the linear stochastic model linearized around (a) the time-mean DJF flow of the 14-level seasonal GCM, (b) the time-mean DJF flow of the ENSO experiment 1982/83, and (c) the difference between (b) and (a). Units are meters.

advantage of this approach is that one loses contact with the underlying dynamical operator. A combination of the two approaches should help us better understand the connections between storm tracks and the mean flow, as well as to appreciate the limitation of the linear stochastic framework.

Acknowledgments. We thank Peter Phillipps for integrating the perpetual insolation GCM, and Paul Kushner, Zuojun Zhang, Isidoro Orlanski, and Steve Garner for assistance in interpreting the linear model results. YZ was supported in part by NOAA Grant NA67RJ0120 to Princeton University.

REFERENCES

Alexander, M. A., and J. D. Scott, 1996: *Atlas of Climatology and Variability in the GFDL R30S14 GCM.* U.S. Government Printing Office, 1996-774-842, 121 pp. [Available from NOAA-CIRES Climate Diagnostics Center, 325 Broadway, Boulder, CO 80303.]

Buizza, R., and T. N. Palmer, 1995: The singular-vector structure of the atmospheric global circulation. *J. Atmos. Sci.,* **52,** 1434–1456.

Christoph, M., U. Ulbrich, and P. Speth, 1997: Midwinter suppression of Northern Hemisphere storm track activity in the real atmosphere and in GCM experiments. *J. Atmos. Sci.,* **54,** 1589–1599.

DelSole, T., 1996: Can quasigeostrophic turbulence be modeled stochastically? *J. Atmos. Sci.,* **53,** 1617–1633.

Farrell, B., and P. Ioannou, 1993a: Stochastic forcing of perturbation variance in unbounded shear and deformation flows. *J. Atmos. Sci.,* **50,** 200–211.

——, and ——, 1993b: Stochastic dynamics of baroclinic waves. *J. Atmos. Sci.,* **50,** 4044–4057.

——, and ——, 1994: A theory for the statistical equilibrium energy spectrum and heat flux produced by transient baroclinic waves. *J. Atmos. Sci.,* **51,** 2685–2698.

——, and ——, 1995: Stochastic dynamics of the midlatitude atmospheric jet. *J. Atmos. Sci.,* **52,** 1642–1656.

——, and ——, 1996a: Generalized stability theory. Part I: Autonomous operators. *J. Atmos. Sci.,* **53,** 2025–2040.

——, and ——, 1996b: Generalized stability theory. Part II: Nonautonomous operators. *J. Atmos. Sci.,* **53,** 2041–2053.

Frederiksen, J. S., 1983: Disturbances and eddy fluxes in Northern Hemisphere flows: Instability of three-dimensional January and July flows. *J. Atmos. Sci.,* **40,** 836–855.

Hoskins, B. J., and P. J. Valdes, 1990: On the existence of storm-tracks. *J. Atmos. Sci.,* **47,** 1854–1864.

Leith, C. E., 1971: Atmospheric predictability and two-dimensional turbulence. *J. Atmos. Sci.,* **28,** 145–161.

Nakamura, H., 1992: Midwinter suppression of baroclinic wave activity in the Pacific. *J. Atmos. Sci.,* **49,** 1629–1642.

Wallace, J. M., G. H. Lim, and M. L. Blackmon, 1988: Relationship between cyclone tracks, anticyclones and baroclinic waveguides. *J. Atmos. Sci.,* **45,** 439–462.

Whitaker, J. S., and P. D. Sardeshmukh, 1998: A linear theory of extratropical synoptic eddy statistics. *J. Atmos. Sci.,* **55,** 237–258.

Zhang, Y., 1997: On the mechanisms of the mid-winter suppression of the Pacific stormtrack. Ph.D. thesis, Princeton University, 152 pp. [Available from NOAA/GFDL, Princeton University, Princeton, NJ 08542-0308.]